



1 **XBT data collected along the Southern Ocean “chokepoint”**
2 **between New Zealand and Antarctica, 1994-2024**

3
4 Giuseppe Aulicino^{*1,2}, Antonino Ian Ferola¹, Laura Fortunato¹, Giorgio Budillon^{1,3}, Pasquale
5 Castagno^{3,4}, Pierpaolo Falco^{3,5}, Giannetta Fusco^{1,3}, Naomi Krauzig^{3,5}, Giancarlo Spezie^{1,3}, Enrico
6 Zambianchi^{1,3}, Yuri Cotroneo^{*1,3}

7
8 ¹ Dipartimento di Scienze e Tecnologie, Università degli Studi di Napoli “Parthenope”, Napoli, 80143, Italy

9 ² Istituto di Scienze Polari, Consiglio Nazionale delle Ricerche, Bologna, 40129, Italy

10 ³ Consorzio Nazionale Interuniversitario per le Scienze del Mare (CoNISMa), Roma, 00196, Italy

11 ⁴ Dipartimento di Scienze Matematiche e Informatiche, Scienze Fisiche e Scienze della Terra, Università degli Studi di
12 Messina, 98122, Italy

13 ⁵ Dipartimento di Scienze della Vita e dell’Ambiente, Università Politecnica delle Marche, Ancona, 60131, Italy

14
15 * *Correspondence to:* Giuseppe Aulicino (giuseppe.aulicino@uniparthenope.it); Yuri Cotroneo
16 (yuri.cotroneo@uniparthenope.it)

17
18
19 **Abstract.** This study presents the water column temperature data collected during several cruises on
20 board the *Italica*, *Araon* and *Laura Bassi* research vessels, in the framework of the Climatic Long-
21 term Interaction for the Mass balance in Antarctica (CLIMA), Southern Ocean Chokepoints Italian
22 Contribution (SOChIC), and Marine Observatory of the Ross Sea (MORSea) projects, funded by the
23 Italian National Antarctic Research Program (PNRA). Data were collected between New Zealand and
24 the Ross Sea during the austral summers from 1994/1995 to 2023/2024. Across this chokepoint of
25 the Antarctic Circumpolar Current, XBT Sippican T7 probes were launched with a regular 20 km
26 sampling, providing temperature profiles with a vertical resolution of 65 cm and a maximum nominal
27 depth of 760 m. All temperature profiles underwent a rigorous quality control, including a general
28 malfunctioning verification, the removal of spikes, the consistency check of adjacent profiles, the
29 comparison to regional oceanographic features and satellite altimetry observations, and a final visual
30 check by operator. Data quality checks led us to discard about 12% of acquired XBT measurements.
31 This dataset contributes to the improvement of our understanding of Southern Ocean features, being
32 highly valuable for studies focusing on climate variability, especially across the Antarctic
33 Circumpolar Current and its fronts. Furthermore, we expect that the collected XBT data will serve as
34 a useful tool for the calibration and validation of recent satellite observations and for the improvement
35 of Southern Ocean oceanographic simulations.



36 **1 Introduction**

37 The temperature of the ocean is one of the key parameters identified by the Global Climate Observing
38 System (GCOS) as being essential for climate studies (World Meteorological Organization, 2016).
39 Together with salinity values, ocean temperatures are necessary to identify and trace the main water
40 masses and monitor their evolution at different spatial and temporal scales.

41 On the larger scales, collecting oceanic temperature and salinity data is of paramount importance to
42 the study of the global thermohaline circulation, which plays a pivotal role in Earth's climate system.
43 The Southern Ocean (SO) plays a fundamental role in this circulation (Gille, 1994; Rintoul, 2018),
44 as some of the global thermohaline circulation "engines" are located near the Antarctic coast,
45 associated with polynya areas (Morales Maqueda et al., 2004; Aulicino & Wadhams, 2022). At
46 smaller scales, temperature data can be used to describe the vertical structure of the ocean (e.g., the
47 thermocline depth and its variability), to locate fronts between different water masses, determine the
48 ocean heat content and volume transport, and to identify meso- and sub-mesoscale ocean dynamics.
49 The main current in the SO is the Antarctic Circumpolar Current (ACC), which is its primary source
50 of heat, nutrients and momentum (Sokolov & Rintoul, 2009a, 2009b). The ACC is one of the largest
51 currents on the planet, flowing from west to east and isolating the Antarctic continent, which makes
52 it strongly dependent on the SO conditions. Additionally, the Antarctic ecosystem is very fragile and
53 temperature-dependent, which highlights the importance of monitoring physical changes in the ocean
54 that surrounds it (Convey & Peck, 2019). Therefore, monitoring the SO and its temperature is
55 essential for improving our knowledge of the processes driving the Antarctic variability and the global
56 climate balance (Rintoul, 2018; Armour et al., 2016).

57 Despite its importance, SO has consistently faced a scarcity of in situ observations due to its remote
58 location and the extreme weather conditions, which often hinder research activities to be carried out
59 on site. The measurements are further limited by the seasonal sea ice presence that inhibits the
60 navigation and the data collection. Additionally, in situ data collection is often conducted with
61 instruments and probes used from ships travelling at their normal speed (e.g., Expendable
62 BathyThermographs – XBT), without the possibility to perform classical full depth CTD casts that
63 require ship stops. The advent of the international ARGO program increased significantly the number
64 of hydrographic observations available in the SO throughout all seasons (Roemmich et al., 2022).
65 However, Lagrangian floats do not allow the collection of information along repeated monitoring
66 lines.

67 Accordingly, many steps have been taken over time to obtain ocean temperature data through remote
68 sensing. Satellite data provide valuable insights about the upper ocean, especially when considering
69 that the surface layer is closely related to fundamental phenomena (e.g., ocean-atmosphere physical



70 and biogeochemical interactions, fronts, currents, meanders, eddies) impacting the large-scale
71 circulation and the meso- and small-scale characteristics of the ocean (e.g., McGillicuddy, 2016;
72 Cotroneo et al., 2016; Seo et al., 2023). Additional information about the water column can also be
73 retrieved from numerical models (e.g., Downes et al., 2015) and 3D reconstructions inferred through
74 machine learning and statistical techniques applied to satellite observations, such as sea surface
75 temperature (e.g., Buongiorno Nardelli et al., 2020). Nonetheless, in-situ measurements are
76 indispensable for achieving the necessary precision and depth coverage. In addition, they provide
77 critical ground-truth for the calibration and validation of satellite retrievals of surface variables, and
78 the improvement of data acquisition algorithms (Aulicino et al., 2022). It is therefore evident that the
79 collection of in-situ data is essential for monitoring ocean temperature.

80 To this aim, the University of Naples Parthenope has been taking part since 1994 in the organization
81 and execution of several oceanographic campaigns along the PX36 monitoring line in the Pacific
82 sector of the SO, i.e., between New Zealand and the Ross Sea, in the framework of the Italian National
83 Antarctic Research Program (PNRA). During each expedition, XBT launches were carried out,
84 collecting ocean temperature data from surface to a maximum of about 760m depth (Falco et al.,
85 2022). This study presents the collected XBT dataset, which significantly contributes to the
86 accessibility of extensive ocean temperature data.

87 In this paper, the methodologies used for data collection and quality control (QC) are described in
88 Section 2; the results and the discussion are reported in Section 3; the data record details and the
89 conclusions are summarized in Section 4.

90



91 **2 Data and methods**

92 **2.1 The XBT dataset**

93 An XBT system is composed of several key components: an expendable ballistic probe that descends
94 into seawater; a data acquisition device that records an electrical signal and converts it into usable
95 numerical data (with the support of a computer unit); a double copper wire that connects the falling
96 probe to the acquisition device (Goni et al., 2019; Parks et al., 2022; Simoncelli et al., 2024). As the
97 probe descends through the water column, temperature measurements are acquired using a Negative
98 Temperature Coefficient (NTC) thermistor mounted on the probe zinc nose, which alters its resistance
99 in response to the seawater temperature it comes into contact with. The insulated copper wire is
100 unwound simultaneously by two spools, i.e., clockwise on the ship and counterclockwise in the falling
101 probe. This technique decouples the XBT vertical descent through the seawater from the ship
102 translational motion (Simoncelli et al., 2024). Data recording continues until the wire breaks or the
103 recording is terminated by the operator. The depth associated with a temperature measurement is not
104 sensed directly because XBT probes do not contain pressure sensors. Instead, it is estimated using a
105 phenomenological Fall Rate Equation (FRE) provided by the manufacturer, with coefficients that
106 vary based on the probe type.

107 The uncertainties on temperature and pressure values make the XBT probe accuracy be generally
108 rated to $\pm 0.10^{\circ}\text{C}$ (Parks et al., 2022), although differences can be retrieved depending on the
109 manufacturer and the manufacturing date of different devices (Cowley and Krummel, 2022).
110 Consequently, some crucial information should be always provided with any XBT dataset for
111 subsequent optimal use of the measurements, including a complete description of the system
112 characteristics in the metadata (e.g., probe type, fall rate coefficients, data originator, platform).

113

114 We present here the dataset of water column temperatures collected in the Pacific sector of the
115 Southern Ocean through XBT casts during several research cruises on board the Italian research
116 vessels “Italica” and “Laura Bassi” and the Korean icebreaker “Araon” (see Table 1). These activities
117 were carried out in the framework of the Italian PNRA by several scientific projects, e.g., Climatic
118 Long-term Interaction for the Mass balance in Antarctica (CLIMA), Southern Ocean observing
119 system and Chokepoints Italian Contribution (SOChIC) and Marine Observatory in the Ross Sea
120 (MORSea).

121 The XBT casts were carried out during the austral summers between 1994/1995 and 2023/2024,
122 mainly in January and February (Figure 1), using Sippican T7 probes providing temperature profiles
123 with a vertical resolution of 65 cm and a maximum nominal depth of 760 m. Only during the
124 1994/1995 (PNRA X) and 1995/1996 (PNRA XI) cruises some Sippican T5 probes were used,



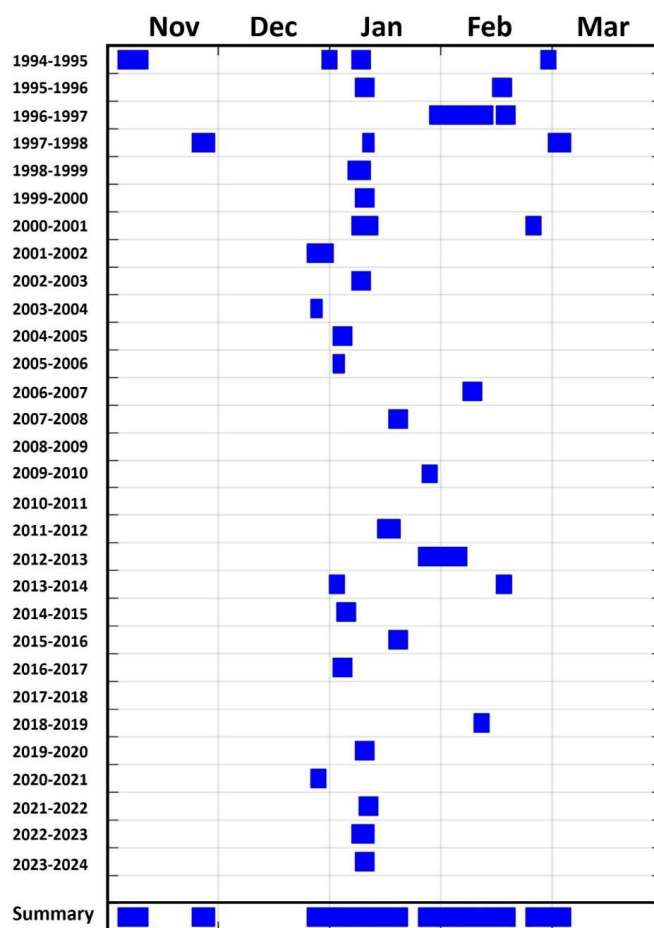
125 reaching a maximum depth of 1830 m, as reported in the campaign metadata information (Table 2).
 126 The majority of transects were completed in 5-6 days and provide a synoptic picture of the thermal
 127 structure of the upper SO across its Pacific Sector (Figure 2). A regular 20 km sampling rate was
 128 adopted with occasional increased sampling frequency over the main frontal regions of the ACC.

129

130 **Table 1.** List of scientific cruises included in this dataset carried out between November 1994 and January 2024

Cruise name	R/V	Start date	End date	Latitude	Longitude
PNRA X	ITALICA	03 November 1994	02 March 1995	47.00 - 74.99°S	172.02°E - 175.90°W
PNRA XI	ITALICA	07 January 1996	18 February 1996	48.66 - 72.01°S	173.56°E - 179.79°E
PNRA XII	ITALICA	26 January 1997	19 February 1997	46.17 - 74.69°S	166.24°E - 179.82°E
PNRA XIII	ITALICA	23 November 1997	06 March 1998	46.25 - 72.71°S	171.39°E - 179.43°W
PNRA XIV	ITALICA	05 January 1999	11 January 1999	48.07 - 69.00°S	173.70°E - 178.55°E
PNRA XV	ITALICA	07 January 2000	18 February 2000	49.17 - 69.83°S	173.13°E - 178.41°E
PNRA XVI	ITALICA	06 January 2001	26 February 2001	48.75 - 75.94°S	170.59°E - 179.72°E
PNRA XVII	ITALICA	24 December 2001	31 December 2001	48.50 - 69.30°S	160.39°E - 178.01°E
PNRA XVIII	ITALICA	06 January 2003	11 January 2003	48.00 - 71.26°S	172.93°E - 177.47°E
PNRA XIX	ITALICA	24 December 2003	28 December 2003	46.36 - 66.17°S	173.81°E - 179.99°E
PNRA XX	ITALICA	01 January 2005	06 January 2005	48.03 - 70.49°S	174.22°E - 178.38°E
PNRA XXI	ITALICA	01 January 2006	04 January 2006	48.03 - 66.50°S	174.59°E - 179.93°E
PNRA XXII	ITALICA	05 February 2007	10 February 2007	47.23 - 71.99°S	170.86°E - 174.26°E
PNRA XXIII	ITALICA	16 January 2008	21 January 2008	47.50 - 68.99°S	174.18°E - 178.63°E
PNRA XXV	ITALICA	25 January 2010	29 January 2010	46.38 - 70.00°S	173.63°E - 178.00°E
PNRA XXVII	ITALICA	13 January 2012	19 January 2012	47.85 - 65.96°S	172.03°E - 176.54°E
PNRA XXVIII	ARAON	24 January 2013	06 February 2013	47.20 - 68.5°S	158.30°E - 177.00°E
PNRA XXIX	ITALICA	30 December 2013	18 February 2014	48.01 - 78.83°S	167.07°E - 175.84°W
PNRA XXX	ARAON	02 January 2015	10 January 2015	47.99 - 73.22°S	157.02°E - 173.81°E
PNRA XXXI	ITALICA	16 January 2016	28 January 2016	47.49 - 72.40°S	171.56°E - 175.00°E
PNRA XXXII	ITALICA	31 December 2016	05 January 2017	48.01 - 68.77°S	174.09°E - 179.85°W
PNRA XXXIV	ARAON	08 February 2019	12 February 2019	47.99 - 69.75°S	166.79°E - 170.87°E
PNRA XXXV	LAURA BASSI	07 January 2020	12 January 2020	48.01 - 69.25°S	172.97°E - 178.84°E
PNRA XXXVI	LAURA BASSI	25 December 2020	02 January 2021	46.96 - 73.39°S	172.82°E - 175.89°E
PNRA XXXVII	LAURA BASSI	08 January 2022	26 January 2022	47.54 - 76.35°S	171.20°E - 177.58°W
PNRA XXXVIII	LAURA BASSI	06 January 2023	12 January 2023	46.56 - 72.27°S	169.40°E - 178.70°E
PNRA XXXIX	LAURA BASSI	07 January 2024	12 January 2024	48.20 - 70.00 °S	166.30 °E – 176.40°E

131



132

133 **Figure 1.** Temporal distribution of the oceanographic campaigns conducted along the New Zealand-Antarctica
 134 “chokepoint” between 1994 and 2024.

135

136 **Table 2.** Characteristics of the different XBT probes used in this study: nominal depth guaranteed by Sippican; maximum
 137 ship speed suggested by Sippican for an optimal drop; coefficient A of Fall Rate Equation $D(t) = At - Bt^2$ used for depth
 138 calculation provided by the manufacturer; amount of ZAMAK, copper and plastic for each probe type (adapted from
 139 Simoncelli et al., 2022)

140

Probe type	Max rated depth (m)	Max ship speed (knots)	FRE coeff A (ms ⁻¹)	FRE coeff B (ms ⁻¹)	ZAMAK (kg)	Plastic (kg)	Copper (kg)
Sippican T5	1830	6	6.828	0.00182	0.613	0.125	0.357
Sippican T7	760	15	6.691	0.00225	0.576	0.052	0.240

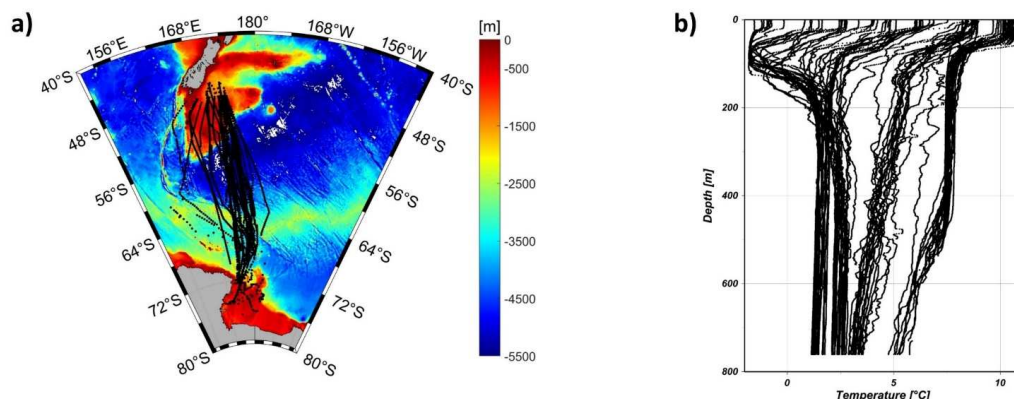
141

142

143



144



145

146 **Figure 2.** a) Map of the Southern Ocean area between New Zealand and Antarctica. The black dots represent the position
147 of all XBT launches carried out between December 1994 and January 2024. b) An example of temperature vertical profiles
148 collected through XBT across the New Zealand – Ross Sea chokepoint during the XXXV Italian Antarctic Expedition.

149

150

151 2.3 Quality Control

152 Various types of malfunctions can affect XBT measurements and result in inaccurate temperature
153 readings within the temperature profile. These faults can appear as a spike in a single recorded value
154 or affect the temperature across a range of depths. Moreover, some issues can create errors that mimic
155 real phenomena, such as temperature inversions or fronts (Parks et al., 2022). Sometimes, profiles
156 can be corrected by deleting or filtering sections of the original data. However, an accurate quality
157 control procedure must be implemented before any data is discarded or manipulated. Additionally, a
158 flagging scheme is generally applied to provide XBT dataset users with quality indicators of the
159 oceanographic data.

160 Quality flags (QFs) are essential for enabling users to filter the XBT dataset according to the specific
161 quality requirements for the intended use. Several flagging scheme exist in agreement with
162 recommendations provided by the Intergovernmental Oceanographic Commission of UNESCO
163 (IOC, 2013). In this study we follow the suggestions provided by the Global Temperature and Salinity
164 Profile Program (GTSP) of the NOAA-NCEI (<https://www.ncei.noaa.gov/products/global-temperature-and-salinity-profile-programme>) resulting in the flagging scheme summarized in Table
165 3 for indicating the quality of each temperature and depth data point.

167

168

169



170 **Table 3.** The Quality Flags (QF) assigned to the XBT data

QF	Quality	Description
0	No QC	No quality control has been performed on this data.
1	Good data	The data is good. No malfunctions have been identified and consistency with real phenomena has been verified.
2	Probably good data	Minor malfunctions present which are small or correctable without affecting overall data quality. Some features (probably real) are present but these are unconfirmed.
3	Probably bad data	Data are suspect and present unusual features which are inconsistent with real phenomena, Data remains potentially correctable.
4	Bad data	The data appears erroneous. Evident errors are identified and there is no likelihood of correction.

171

172

173 The assignment of QFs is the result of a series of quality control (QC) tests for both temperature and
174 depth data which are used to get a reliable quality check of the temperature measurements collected
175 through our XBTs and of the retrieved depths. Results of each test allowed to insert the relative flag
176 to the corresponding measurement according to the scheme shown in Table 3. QF=1 is assigned when
177 all the tests pass and QF=4 when at least one test fails. For temperature, more detailed checks are
178 performed, including a final visual check, allowing us to introduce QF=2 and QF=3 for probably
179 good and probably bad data, respectively (as detailed below).

180 Overall, the QC procedures applied to our dataset follow recommendations previously suggested by
181 NOAA, developed and refined in the last three decades (Bailey et al., 1994; Daneshzadeh et al., 1995;
182 Cowley and Krummel, 2022; Parks et al., 2022; Tan et al., 2023). These procedures include several
183 steps undertaken in a top-down manner, as temperature data are measured from the surface down,
184 and faults that occur at a given depth may impact on deeper data (Parks et al., 2022).

185 First, each XBT profile was tested for invalid metadata information, such as the correct time, cast
186 position and any other possible operator errors, using a sequence of independent checks. All identified
187 errors in date and time were corrected accordingly, with the support of the XBT launch clipboards
188 provided by operators on board. No errors were found concerning the position of the casts after the
189 comparison of latitudes and longitudes against gridded GEBCO 2 x 2 minutes bathymetry (GEBCO
190 Compilation Group, 2023). The check of unrealistic positions was also performed using the
191 calculation of vessel speed from profile date and time and an upper general threshold of 20 knots
192 (since most of the launches are realized by ships travelling in the range of 10/15 knots). Additionally,
193 the depth values of each XBT profile were compared to the last good depth value provided by the
194 operators (QF=1 is assigned to shallower depth values, otherwise they are flagged as QF=4).



195 Then, all the vertical temperature profiles were checked for nominal maximum depth (760 m), and
196 carefully inspected to identify malfunctions, coherence to regional oceanographic features, drop-to-
197 drop consistency along the cruise track, and presence of unusual features. In this context, the main
198 difficulty is usually found in distinguishing a common malfunction from a regional oceanographic
199 feature (i.e., unexpected increase of temperature southward or along the water column).
200 Consequently, unusual features were cross-validated by comparison to repeated (within 15 minutes)
201 or neighbouring profiles from the same voyage and eventually to available Austral summer ARGO
202 observations over the study area. To this aim, we took again advantage of XBT launch clipboards, in
203 which operators notified any instrument malfunctions, adverse weather conditions, sea ice presence
204 and local bottom depth. In particular, the bottom depth was relevant to constraining XBT data profiles
205 at the right elevations, especially when approaching shallow waters (QF=1 is assigned to values
206 shallower than bottom depth, otherwise they are flagged as QF=4). When the clipboard was not
207 available, we relied instead on the GEBCO 2 x 2 minutes bathymetry (GEBCO et al., 2023), which
208 resulted the most correspondent to the in situ reported depths over the area and period of study.
209 Additionally, a gross filter was applied to all the XBT profiles using a series of temperature thresholds
210 that vary on four vertical layers, as reported in Table 4. The thresholds were defined through the use
211 of ARGO data collected in the study area between 2004 and 2023. QF=4 was applied to data
212 exceeding the thresholds of $\pm 0.5^{\circ}\text{C}$.

213

214 **Table 4.** Temperature thresholds applied to XBT profiles, defined in four levels.

Depth range (m)	Temperature minimum ($^{\circ}\text{C}$)	Temperature maximum ($^{\circ}\text{C}$)
0 - 100	-1.866	14.698
100 - 250	-1.865	11.093
250 - 500	0.068	8.717
500 - 760	0.826	8.266

215

216

217 Several studies assess that the XBT measurements near the sea surface may be considered unreliable
218 due to the stabilization of motion and thermal adaptation to the surrounding environment (e.g. Bailey
219 et al., 1994; Cowley and Krummel, 2022; Simoncelli et al., 2024). They also suggest that the first
220 acceptable value is at about 4 m depth and that the data user must be carefully informed in order to
221 exclude suspect surface values from scientific analyses. Here, we opted for providing all the original
222 measurements annotating their quality, as resulting from a dedicated test on the initial part of each
223 profile. This test calculates the differences between the value recorded at time $t = 0.6$ s (about 4 m



224 depth) and shallower measurements, classifying them based on the standard uncertainty on
225 temperature attributable to an XBT probe ($0.10\text{ }^{\circ}\text{C}$) as a metric (Simoncelli et al., 2024). Therefore,
226 temperature data are assigned QF=1 if the difference is less than or equal to standard deviation (std);
227 QF=2 if it is comprised between std and $2*\text{std}$; QF=3 if it is comprised between $2*\text{std}$ and $3*\text{std}$; and
228 QF=4 if it is higher than $3*\text{std}$.

229 Then, the XBT profiles were examined for the presence of spikes, unrealistic oscillations and
230 unusually gradients in temperature data, as well as sharp variations toward negative or higher values,
231 which could be caused by copper wire breaks. Data are mostly flagged as good (QF=1) or bad (QF=4)
232 values. Nonetheless, suspect data are compared with neighbouring profiles and ARGO climatology
233 over the study area, eventually assigning QF=1, QF=2 and QF=3 attributes. For example, QF=2 is
234 used when an XBT profile presents a step-like feature that is not confirmed by a neighbouring profile
235 but is consistent with similar features previously observed in the study region. QF=3 is used, instead,
236 when XBT values exhibit suspect temperature values that cannot be confirmed by a neighbouring
237 profile and occur in areas where there is no evidence of mesoscale structures (e.g., eddies or fronts).
238 Nevertheless, an increase or decrease in temperature over large depth ranges compared to
239 neighbouring profiles, can be also associated to an eddy, a frontal area or an intense current system.
240 Therefore, QF=1 is applied when repeated profiles showing similar temperatures or archive data can
241 confirm the feature. The larger scale description of ocean dynamics obtained through satellite
242 altimetry was also used for controversial results to identify the presence of eddies and frontal systems
243 affecting the temperature data.

244 However, some profiles might exhibit anomalous features that the described QC procedure could not
245 detect as erroneous values. Therefore, an additional visual check was carried out for each individual
246 cruise track and each vertical temperature profile to verify the assigned QF=2 and QF=3 flags and
247 identify any residual anomalies in the positioning of the XBT launches or outliers in the data
248 collection. This control was performed using the Ocean Data View (ODV) software (Schlitzer, 2023).
249 Overall, the entire QC led us to discard about 12% of acquired XBT observations, which were flagged
250 as bad or probably bad data (Figure 3).

251
252

2.4 XBT data biases correction

253 Previous studies assessed that temperature biases and depth errors, due to inaccurate time conversion
254 to depth through FRE, may affect XBT observations (e.g., Gouretski and Reseghetti, 2010; Cowley
255 et al., 2013). Although a full comprehension of the origins of these issues is still pending, several
256 experiments tried to quantify this bias by comparing XBT profiles with co-located CTD observations,
257 demonstrating that XBT temperatures are usually warmer than reality (Gouretski and Reseghetti

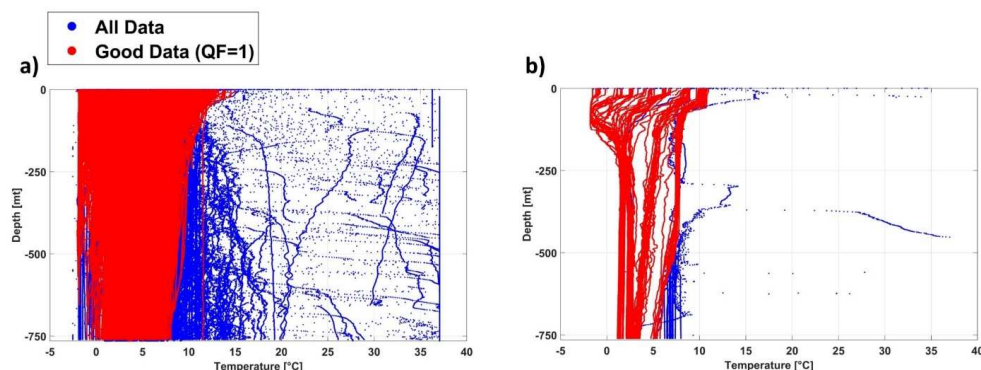


258 2010; Cheng et al., 2014). Different possible causes of biases emerged, including mechanical (e.g.,
259 probe type, manufacturer, year), external (e.g., launch height, meteo-marine conditions) and electrical
260 (e.g., thermistor, wire) factors (Seaver and Kuleshov 1982; Green, 1984; Reverdin et al. 2009).
261 Additionally, a decrease in fall rate was observed in cooler waters because of increased viscosity
262 (Gouretski and Reseghetti 2010), making FRE corrections in the Southern Ocean extremely important
263 (Cheng et al., 2014).

264 To address these problems, several correction schemes have been proposed over the past few decades.
265 A comprehensive list of related papers is available at [https://www.ncei.noaa.gov/products/xbt-](https://www.ncei.noaa.gov/products/xbt-corrections)
266 [corrections](https://www.ncei.noaa.gov/products/xbt-corrections). Taking advantage of more than 220,000 XBT-CTD side-by-side pairs, Cheng et al.
267 (2014) examined and compared existing methodologies, proposing a new correction scheme for
268 historical XBT data for nine independent probe-type groups. Their study confirmed that depth error
269 and pure temperature bias are temperature-dependent and may be influenced by the data acquisition
270 and recording system. Moreover, the resulting scheme also considers that some biases affecting the
271 XBT-derived temperature profiles vary with manufacturer/probe type and have been shown to be
272 time dependent, and that depth correction varies with depth (Cheng et al. 2016).

273 In our dataset, we apply this methodology, which includes corrections for both temperature and depth
274 values based on calendar year, water temperature, and probe type, to provide bias-corrected XBT
275 measurements (Cheng et al., 2014). A full description of the methodology and an update table of
276 applied coefficients are available at https://www.nodc.noaa.gov/OC5/XBT_BIAS/ch-method.html
277 and <http://www.ocean.iap.ac.cn/pages/dataService/dataService.html?navAnchor=dataService>.

278
279




280
281
282
283
284
285

Figure 3. a) XBT observations collected between December 1994 and January 2024 over the New Zealand – Ross Sea
chokepoint before (blue) and after (red) the quality check; b) An example of the quality check on the XBT data collected
during the XXXV PNRA cruise.

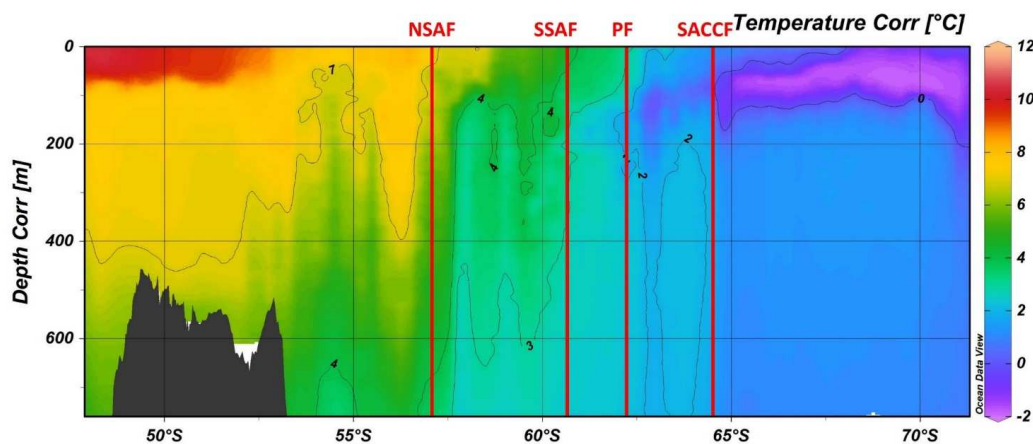


286 **3. Results and discussion**

287 We believe this exceptional temperature dataset provides a valuable reservoir of high-resolution,
288 independent, and trustworthy information. The dataset assumes notable significance, representing an
289 extensive temporal series of data collected nearly every austral summer over the last 30 years, within
290 the same oceanic sector of the SO and along the same monitoring transect (PX36). We exploited this
291 information to provide 36 vertical sections of the ocean temperature, from the surface to about 800 m
292 depth, along the New Zealand–Antarctica “chokepoint”. Figures representing the latitudinal sections
293 of corrected XBT temperatures during each leg are available in the supplementary information
294 (Figures S1) .

295 The repeated temperature sections significantly enhance our understanding of ACC fronts and their
296 evolution over the last three decades. A first application of the dataset is shown in Figure 4 where
297 XBT observations collected during the XVIII PNRA expedition are used for the identification of the
298 main ACC fronts positions: Northern Sub Antarctic Front (NSAF); Southern Sub Antarctic Front
299 (SSAF); Polar Front (PF); Southern Antarctic Circumpolar Current (sACCF). The criteria used for
300 identifying the fronts (Table 5) follow Budillon and Rintoul (2003), which compiles several
301 hydrographic definitions (Botnikov, 1963; Belkin, 1990; Orsi et al., 1995; Rintoul et al., 1997). The
302 **SBdy** of the ACC, usually described as the maximum southern extent of vertical maximum of
303  .5°C at about 200 m (Orsi et al., 1995), is not described in this sector as its position is coincident
304 with the sACCF position in most of the available temperature sections.

305



306

307 **Figure 4.** Temperature vertical section from XBT data collected during the XVIII PNRA expedition along the New
308 Zealand–Antarctica “chokepoint” in which the vertical red lines represent the ACC main fronts positions: Northern Sub
309 Antarctic Front (NSAF); Southern Sub Antarctic Front (SSAF); Polar Front (PF); Southern Antarctic Circumpolar Front
310 (SACCF). The dark grey mask represents the bathymetry.

311



312

313 **Table 5.** Criteria for front definitions (Adapted from Budillon & Rintoul, 2003)

Front	Definition	Reference
Southern Antarctic Circumpolar Current Front (sACCF)	$T > 1.8^{\circ}\text{C}$ along the T_{max} at depth > 500 m, farther north; $T < 0^{\circ}\text{C}$ along the T_{min} at depth < 150 m, farther south.	Orsi <i>et al.</i> 1995.
Polar Front (PF)	$T < 2^{\circ}\text{C}$ at 200 m, farther south.	Botnikov 1963, Orsi <i>et al.</i> 1995.
Subantarctic Front (SAF)	Maximum temperature gradient in the range $3\text{--}8^{\circ}\text{C}$ at 300 m.	Belkin 1990.
Northern Sub-Antarctic Front (NSAF)	Maximum temperature gradient in the range $4\text{--}7^{\circ}\text{C}$ at 300 m.	Rintoul <i>et al.</i> 1997.
Southern Sub-Antarctic Front (SSAF)	Maximum temperature gradient in the range $3\text{--}4^{\circ}\text{C}$ at 300 m.	Rintoul <i>et al.</i> 1997.

314

315

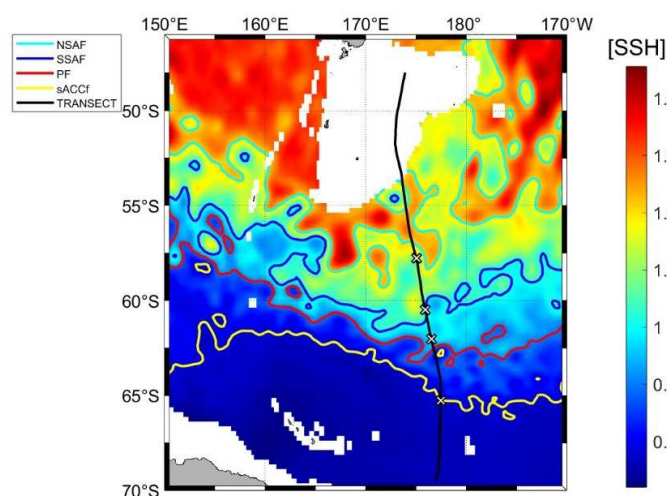
316 The ACC fronts positions retrieved through XBT data also serve as ground truth for the validation of
317 those retrieved through satellite altimetry (e.g., Sokolov and Rintoul 2009a, 2009b; Graham et al.,
318 2012; Chapman, 2017), thereby enhancing the identification process of fronts within the SO. This is
319 extremely desirable in region characterized by **significant influenced** by topographic steering, such
320 as the area south of New Zealand where the presence of the Campbell Plateau severely affects the
321 ACC path (Figure 5). To point out differences and similarities between ACC fronts positions
322 identified through XBT and satellite observations, in Figure 5 we present a Sea Surface Height (SSH)
323 map of the study area, averaged over the period covered by the temperature section in Figure 4 (about
324 7 days). To identify the ACC fronts from satellite data, we applied the SSH isolines methodology that
325 associates a specific value of SSH with each front. For the selection of these values, we relied on
326 previous studies (Sokolov and Rintoul 2007, 2009a, 2009b) proving that the multiple jets of ACC
327 fronts are consistently aligned with streamlines identified by nearly constant circumpolar values of
328 SSH contours.

329 Furthermore, ACC fronts exhibit instabilities that give rise to the generation of eddies.
330 Eddies, characterized as vortices pervading the ocean, assume a pivotal role, particularly within the
331 SO, contributing significantly to the transfer of heat, nutrients, and momentum (e.g., Chelton et al.
332 2011a; Falco and Zambianchi, 2011; Cotroneo et al., 2013; Trani et al., 2014; Rintoul, 2018; Menna
333 et al., 2020). While altimetry proves valuable in gaining insights into surface eddy dynamics, it cannot
334 provide information regarding vertical temperature variations within the eddy structure. Through the
335 temperature sections derived from XBT data, we can discern the presence or absence of an eddy and
336 get basic observations for the analysis of its heat content.

337 An example is provided in Figure 6 where we present the latitudinal section of temperatures observed
338 during the return leg of the 2013-2014 Italian Antarctic expedition (PNRA XXIX). This section shows

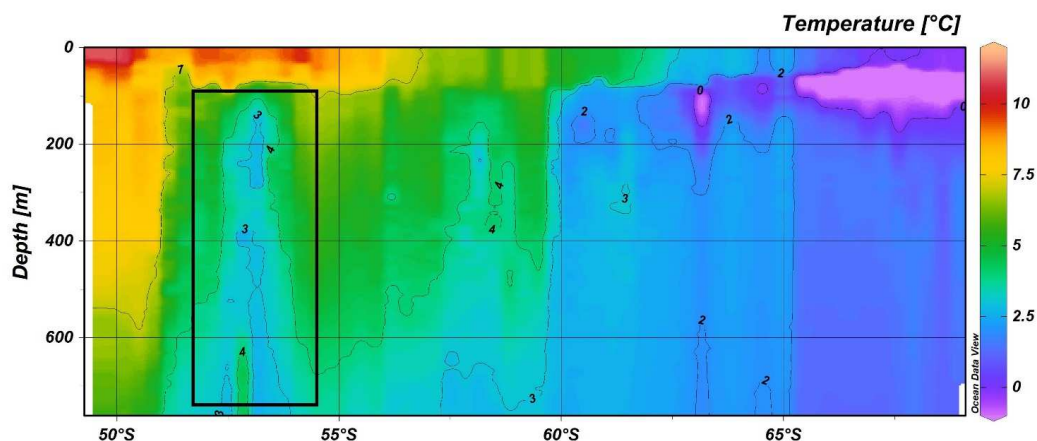


339 the intrusion of a cold core eddy at about 53°S, next to the Campbell Plateau edge. The eddy is
340 characterized by a maximum negative temperature anomaly (eddy's core) of about -4°C with respect
341 to the surrounding water. This negative anomaly results in the formation of a depression in the SSH,
342 also detectable in satellite imagery. In the SSH map shown in Figure 7, the cold core eddy is identified
343 as a closed circle of the blue isoline associated with the SSAF.
344

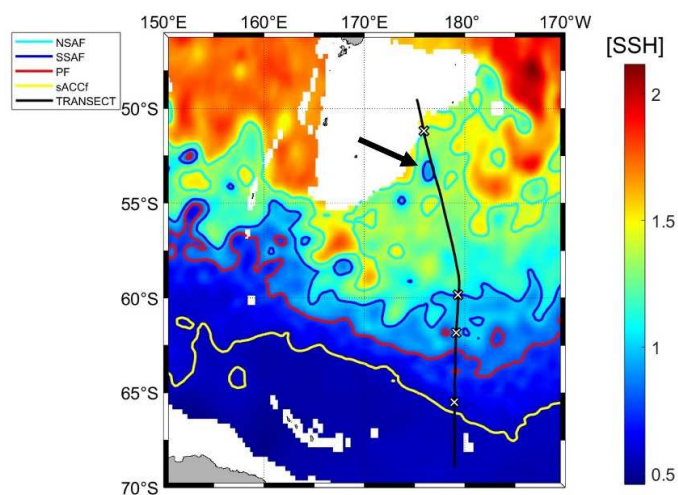


345
346 **Figure 5.** Altimetric map of SSH mediated throughout the XVIII PNRA expedition along the PX36 monitoring line.
347 Contours of different colours identify the position of the main fronts of the ACC retrieved through SSH: NSAF in cyan;
348 SSAF in blue; PF in red and sACCf in yellow. White crosses represent the position of the fronts derived from XBT data.
349 The ship's route is represented by the black line.
350

351 Generally, the combined use of in situ observations and satellite data is crucial as it prevents errors
352 in front positioning and eddy identification. Strong horizontal temperature gradients, often linked to
353 eddies, could be misinterpreted as ACC fronts. Similarly, this approach allows us to distinguish eddies
354 from other mesoscale structures, a difficult task when relying only on altimetry. XBT and satellite
355 information are also complementary in providing valid terms of comparison, at different temporal
356 and spatial scales (XBT at fine-scale; altimetry at meso- and large-scale), for numerical model
357 products representing ocean circulation and eddies dynamics (e.g., Chen X. et al., 2024; Chen Z. et
358 al., 2024).
359



360
361 **Figure 6.** Temperature vertical section from XBT data collected during the XXIX PNRA expedition along the New
362 Zealand–Antarctica “chokepoint” in which the black box identifies the position of an ACC’s cold core eddy.
363



364
365 **Figure 7.** Altimetric map of SSH mediated throughout the XXIX PNRA expedition along the PX36 monitoring line.
366 Contours of different colours identify the position of the main fronts of the ACC retrieved through SSH: NSAF in cyan;
367 SSAF in blue; PF in red and sACCf in yellow. White crosses represent the position of the fronts derived from XBT data.
368 The ship's route is represented by the black line. The black arrow indicates the observed cold core eddy.
369

370 4. Data availability

371 XBT data are publicly accessible in text format files through the NOAA-NCEI unrestricted
372 repositories, as listed in Table 6. NCEI (National Centers for Environmental Information) serves as
373 the official archive for data, metadata, and products collected and provided by NOAA (National



374 Oceanic and Atmospheric Administration). NCEI also hosts quality checked data by non-NOAA
 375 scientists and is regarded as one of the world’s most comprehensive ocean, atmospheric and
 376 geophysical archives, with over 60 petabytes of data covering the full range of Earth’s environmental
 377 systems and cycles.

378 Each XBT file includes the main variables summarized in Table 7, the relative metadata (i.e., probe
 379 type, software, manufacturer, fall rate coefficients, data originator, scientific project, platform) and a
 380 short description of the dataset. One file is created for each research cruise. The naming convention
 381 is xbt_ship_cruise_all_QC, where ship and cruise are identification names of the research vessel used
 382 for the XBT launch and the PNRA research expedition number, respectively, as in Table 1.

383

384 **Table 6.** XBT data repository list

Data set	DOI	Reference
PNRA X – 1st leg	https://doi.org/10.7289/v5rf5s9v	Cotroneo et al., 2018a
PNRA X – 2nd leg	https://doi.org/10.7289/v53r0r5z	Cotroneo et al., 2018b
PNRA XI	https://doi.org/10.7289/v5x065b9	Cotroneo et al., 2018c
PNRA XII	https://doi.org/10.7289/v5kd1w6b	Cotroneo et al., 2018d
PNRA XIII	https://doi.org/10.7289/v50863mf	Cotroneo et al., 2018e
PNRA XIV	https://doi.org/10.7289/v5mg7mtc	Cotroneo et al., 2018f
PNRA XV	https://doi.org/10.7289/v56d5r8p	Cotroneo et al., 2018g
PNRA XVI	https://doi.org/10.7289/v5s75dpg	Cotroneo et al., 2018h
PNRA XVII	https://doi.org/10.7289/v5ng4nzt	Cotroneo et al., 2018i
PNRA XVIII	https://doi.org/10.7289/v5qz289c	Cotroneo et al., 2018j
PNRA XIX	https://doi.org/10.7289/v5vq3113	Cotroneo et al., 2018k
PNRA XX	https://doi.org/10.7289/v5vh5m45	Cotroneo et al., 2018l
PNRA XXI	https://dx.doi.org/10.25921/hzcp-d813	Cotroneo et al., 2019
PNRA XXII	https://doi.org/10.25921/c8bm-xh74	Cotroneo et al., 2018m
PNRA XXIII	https://doi.org/10.25921/q29v-c980	Cotroneo et al., 2018n
PNRA XXV	https://doi.org/10.7289/v50r9mmm	Cotroneo et al., 2017 ^o
PNRA XXVII	https://doi.org/10.7289/v54j0cbw	Cotroneo et al., 2017b
PNRA XXVIII	https://doi.org/10.25921/9YTS-P771	Cotroneo et al., 2018o
PNRA XXIX	https://doi.org/10.25921/220j-b370	Cotroneo et al., 2024a
PNRA XXX	https://doi.org/10.25921/9ph6-c102	Cotroneo et al., 2024b
PNRA XXXI	https://doi.org/10.25921/zf04-ch06	Cotroneo et al., 2024c
PNRA XXXII	https://doi.org/10.25921/vvmp-rr55	Cotroneo et al., 2024d
PNRA XXXIV	https://doi.org/10.25921/jeez-zf77	Cotroneo et al., 2024e
PNRA XXXV	https://doi.org/10.25921/lysg-dw94	Cotroneo et al., 2024f
PNRA XXXVI	https://doi.org/10.25921/aeg5-hw87	Cotroneo et al., 2024g
PNRA XXXVII	https://doi.org/10.25921/3mmd-tj60	Cotroneo et al., 2024h
PNRA XXXVIII	https://doi.org/10.25921/kte7-d058	Cotroneo et al., 2024i
PNRA XXXIX	https://doi.org/10.25921/jc13-ek97	Cotroneo et al., 2024l



385

386 **Table 7.** Name and description of the main variables included in the XBT text files.

Name of variable	Unit	Description
Cruise		Cruise name
Station		Identifier number of XBT deployment
Time	dd/mm/yyyy hh:mm	Date and time of XBT deployment
Latitude [degrees_north]	Decimal degree	Latitude of XBT deployment
Longitude [degrees_east]	Decimal degree	Longitude of XBT deployment
Temperature [°C]	Celsius degree	XBT temperature measurements
Depth [m]	Meters	Depth of the XBT temperature measurements
Bot. Depth [m]	Meters	Maximum depth of XBT measurements
QF	0 - 4	Quality flags of XBT measurements
Temperature Corr. [°C]	Celsius degree	Corrected XBT temperature measurements
Depth Corr. [m]	Meters	Corrected depth of the XBT temperature measurements

387

388

389 5. Conclusions

390 The SO is a key place for atmosphere–ocean physical and biogeochemical interactions at different
391 spatial and temporal scales (Falco and Zambianchi, 2011; Cerrone et al., 2017a, b; Buongiorno
392 Nardelli et al., 2017). However, despite their importance, processes in many areas of the SO are still
393 poorly known due to the scarcity of in situ measurements. This is particularly true for the ACC region
394 and its fronts, which are characterized by complex dynamics and intense eddy activity (Trani et al.,
395 2011; Cotroneo et al., 2013; Frenger et al., 2015, Menna et al., 2020; Ferola et al., 2023). To fill this
396 gap, all available measurements provide a significant contribution and should be shared within the
397 oceanographic community.

398 To this goal, here we present 36 vertical sections of XBT ocean temperature data collected between
399 New Zealand and the Ross Sea (PX36 line) during the Austral summers from 1994/1995 to
400 2022/2023. This dataset provides direct insights into the 0-800 m thermal characteristics of the Pacific
401 sector of the SO and complements data sourced from observing networks, drifters, ARGO floats and
402 glider fleets. It is also suitable to be combined with enhanced spatial and temporal scale remotely
403 sensed observations and numerical simulations. This comprehensive dataset lays a robust foundation
404 for a nuanced analysis of the key mechanisms governing thermohaline circulation in the SO and for
405 improving our knowledge of the physical and biogeochemical characteristics of the four-dimensional
406 ocean.

407 The continuation of this XBT collection over time, in the framework of the Italian PNRA research
408 expeditions to Antarctica, is particularly important due to the inherent challenges associated with data



409 acquisition in the SO and promises an increasingly comprehensive and detailed understanding of
410 thermal variations in this specific maritime region.

411

412 **Author contributions.** GA, YC and AIF conceived and designed the manuscript. GA, YC, PC, PF, GF, GB, NK, GS, EZ and
413 AIF collected the measurements and organized the XBT dataset. GA, YC, LF and AIF carried out the quality control analyses. All
414 authors analysed the achieved results, contributed to the writing, and approved the final manuscript.

415

416 **Competing interests.** The authors declare that they have no conflict of interest.

417

418 **Acknowledgements.** This study was made possible thanks to the contribution of the Climatic Long-term Interaction for the
419 Mass balance in Antarctica (CLIMA), Southern Ocean Chokepoints Italian Contribution (SOChIC), Marine Observatory of the Ross
420 Sea (MORSea), Effects of the east current on the Salinity variability in the Ross Sea (ESTRO) and Physical and biogeochemical tracing
421 of water masses at source areas and export gates in the Ross Sea and impact on the Southern Ocean (SIGNATURE) projects, part of
422 the Italian National Antarctic Research Program (PNRA). Special thanks go to Arturo De Alteris, Massimo De Stefano and Giovanni
423 Zambardino who provided essential support to data acquisition, as well as to the captain, officers, and crew of the research vessels used
424 for XBT launches.

425

426

427 References

428

429 Armour, K.C., Marshall, J., Scott, J.R., Donohoe, A. and Newsom, E.R.: Southern Ocean warming
430 delayed by circumpolar upwelling and equatorward transport, *Nat. Geosci.*, 9, 549–554,
431 <https://doi.org/10.1038/ngeo2731>, 2016.

432

433 Aulicino, G. and Wadhams, P.: Editorial for the Special Issue “Remote Sensing of the Polar Oceans”.
434 *Remote Sens.*, 14, 6195, <https://doi.org/10.3390/rs14246195>, 2022.

435

436 Aulicino, G., Cotroneo, Y., de Ruggiero, P., Buono, A., Corcione, V., Nunziata, F., Fusco, G.: Remote
437 Sensing Applications in Satellite Oceanography, In P. Daponte et al. (eds.), *Measurement for the Sea*,
438 Springer Series in Measurement Science and Technology, http://dx.doi.org/10.1007/978-3-030-82024-4_8, 2022.

439

440
441 Bailey, R., Gronell, A., Phillips, H., Tanner, E., and Meyers, G.: Quality control cookbook for XBT
442 data, Version 1.1. CSIRO Marine Laboratories Reports, 221, <https://doi.org/10.25607/OBP-1482>,
443 1994.

444

445 Belkin, I. M. and Gordon, A. L.: Southern Ocean fronts from the Greenwich meridian to Tasmania,
446 *J. Geophys. Res.*, 101, <https://doi.org/10.1029/95JC02750>, 1996.

447

448 Botnikov, V. N.: Geographical position of the Antarctic Convergence Zone in the Antarctic
449 Ocean, *Soviet Antarctic Exped. Inform. Bull.*, 41, 324-327, 1963.

450

451 Budillon, G. and Rintoul, S. R.: Fronts and upper ocean thermal variability south of New Zealand,
452 *Antartct. Sci.*, 15, 141-152, <https://doi.org/10.1017/S0954102003001135>, 2003.

453

454 Buongiorno Nardelli, B., Guinehut, S., Verbrugge, N., Cotroneo, Y., Zambianchi, E., and Iudicone,
455 D.: Southern Ocean mixed-layer seasonal and interannual variations from combined satellite and in
456 situ data, *J. Geophys. Res.: Oceans*, 122(12), <https://doi.org/10.1002/2017JC013314>, 2017.

457



- 458 Buongiorno Nardelli, B.: A Deep Learning Network to Retrieve Ocean Hydrographic Profiles from
459 Combined Satellite and In Situ Measurements, *Remote Sens.*, 12, 3151.
460 <https://doi.org/10.3390/rs12193151>, 2020.
461
- 462 Cerrone, D., Fusco, G., Cotroneo, Y., Simmonds, I., and Budillon, G.: The Antarctic circumpolar
463 wave: Its presence and interdecadal changes during the last 142 years, *J. Climate*, 30(16), 6371–6389,
464 <https://doi.org/10.1175/JCLI-D-16-0646.1>, 2017a.
465
- 466 Cerrone, D., Fusco, G., Simmonds, I., Aulicino, G., and Budillon, G.: Dominant covarying climate
467 signals in the Southern Ocean and Antarctic sea ice influence during the last three decades. *J. Climate*,
468 30(8), 3055–3072, <https://doi.org/10.1175/JCLI-D-16-0439.1>, 2017b.
469
- 470 Chelton, D. B., Schlax, M. G., Samelson, R. M.: Global observations of nonlinear mesoscale eddies,
471 *Prog. Oceanogr.*, Volume 91, Issue 2, 167-216, <https://doi.org/10.1016/j.pocean.2011.01.002>, 2011.
472
- 473 Chen, Z., Wang, X., Cao, H., Song, X.: Mapping high-resolution surface current by incorporating
474 geostrophic equilibrium with surface quasigeostrophic theory using multi-source satellite
475 observations, *Remote Sens. Environ.*, 304, <https://doi.org/10.1016/j.rse.2024.114058>, 2024.
476
- 477 Chen, X., Chen, G., Ge, L., Cao, C. and Huang, B.: Medium-range forecasting of oceanic eddy
478 trajectory, *Int. J. Digit. Earth*, 17:1, <https://doi.org/10.1080/17538947.2023.2300325>, 2024.
479
- 480 Cheng, L., J. Zhu, R. Cowley, T. Boyer, and S. Wijffels: Time, probe type, and temperature variable
481 bias corrections to historical expendable bathythermograph observations. *J. Atmos. Oceanic
482 Technol.*, 31, 1793-1825, <https://doi.org/10.1175/Jtech-D-13-00197.1>, 2014.
483
- 484 Cheng, L., Abraham, J., Goni, G., Boyer, T., et al.: XBT Science: assessment of instrumental biases
485 and errors, *Bulletin of the American Meteorological Society*, 97, 924-933.
486 <http://dx.doi.org/10.1175/BAMS-D-15-00031>, 2016.
487
- 488 Convey, P., and Peck, L. S.: Antarctic environmental change and biological responses, *Sci. Adv.*,
489 <https://doi.org/10.1126/sciadv.aaz0888>, 2019.
490
- 491 Cotroneo, Y., Budillon, G., Fusco, G. and Spezie, G.: Cold core eddies and fronts of the Antarctic
492 Circumpolar Current south of New Zealand from in situ and satellite data, *J. Geophys. Res.
493 Oceans*, 118, 2653–2666, <https://doi.org/10.1002/jgrc.20193>, 2013.
494
- 495 Cotroneo, Y., Aulicino, G., Ruiz, S., Pascual, A., Budillon, G., Fusco, G., and Tintoré, J.: Glider and
496 satellite high resolution monitoring of a mesoscale eddy in the Algerian basin: Effects on the mixed
497 layer depth and biochemistry, *J. Mar. Syst.*, 162, 73-88,
498 <https://doi.org/10.1016/j.jmarsys.2015.12.004>, 2016.
499
- 500 Cotroneo, Y., Budillon, G., Artegiani, A., Conversano, F., Corbo, C., Gallarato, A., et al.: Water
501 temperature data from XBT taken from the research vessel *Italica* in the Southern Ocean and
502 Southwest Pacific Ocean from 1994-11-03 to 1995-01-01 (NCEI Accession 0170608), NOAA
503 National Centers for Environmental Information. <https://doi.org/10.7289/v5rf5s9v>, 2018a.
504



505 Cotroneo, Y., Budillon, G., Artegiani, A., Conversano, F., Corbo, C., Gallarato, A., et al.: Water
506 temperature data from XBT taken from the research vessel *Italica* in the Southern Ocean and
507 Southwest Pacific Ocean from 1995-01-06 to 1995-03-02 (NCEI Accession 0170765), NOAA
508 National Centers for Environmental Information. <https://doi.org/10.7289/v53r0r5z>, 2018b.

509
510 Cotroneo, Y., Budillon, G., Artegiani, A., Ferrara, C., Meloni, R., & Spezie, G.: Water temperature
511 from XBT taken from research vessel *Italica* in the Southern Ocean and Southwest Pacific Ocean
512 from 1996-01-07 to 1996-02-18 (NCEI Accession 0171481), NOAA National Centers for
513 Environmental Information. <https://doi.org/10.7289/v5x065b9>, 2018c.

514
515 Cotroneo, Y., Budillon, G., Conversano, F., Ferrara, C., & Spezie, G.: Water temperature from XBT
516 taken from the research vessel *Italica* in the Southern Ocean and Southwest Pacific Ocean from 1997-
517 01-26 to 1997-02-19 (NCEI Accession 0172042), NOAA National Centers for Environmental
518 Information. <https://doi.org/10.7289/v5kd1w6b>, 2018d.

519
520 Cotroneo, Y., Budillon, G., Bergamasco, A., Capello, M., De Stefano, M., Ferrara, C., et al.: Water
521 temperature data from XBT collected from research vessel *Italica* in Southern Ocean and Southwest
522 Pacific Ocean from 1997-11-23 to 1998-03-06 (NCEI Accession 0172859). NOAA National Centers
523 for Environmental Information. <https://doi.org/10.7289/v50863mf>, 2018e.

524
525 Cotroneo, Y., Budillon, G., Ferrara, C., Meloni, R., Paschini, E., & Spezie, G.: Water temperature
526 from XBT taken from the research vessel *Italica* in the Southern Ocean and Southwest Pacific Ocean
527 from 1999-01-05 to 1999-01-11 (NCEI Accession 0173211), NOAA National Centers for
528 Environmental Information. <https://doi.org/10.7289/v5mg7mtc>, 2018f.

529
530 Cotroneo, Y., Budillon, G., Ferrara, C., Paschini, E., Russo, A., & Spezie, G.: Water temperature from
531 XBT taken from the research vessel *Italica* in the Southern Ocean and Southwest Pacific Ocean from
532 2000-01-07 to 2000-02-18 (NCEI Accession 0173212), NOAA National Centers for Environmental
533 Information. <https://doi.org/10.7289/v56d5r8p>, 2018g.

534
535 Cotroneo, Y., Budillon, G., Bergamasco, A., De Stefano, M., Ferrara, C., Paschini, E., & Spezie, G.:
536 Water temperature from XBT taken from the research vessel *Italica* in the Southern Ocean and
537 Southwest Pacific Ocean from 2001-01-06 to 2001-02-26 (NCEI Accession 0173213), NOAA
538 National Centers for Environmental Information. <https://doi.org/10.7289/v5s75dpg>, 2018h.

539
540 Cotroneo, Y., Budillon, G., Ferrara, C., Orsi, M., Paschini, E., Rivaro, P., & Spezie, G.: Water
541 temperature from XBT taken from the research vessel *Italica* in the Southern Ocean and Southwest
542 Pacific Ocean from 2001-12-24 to 2001-12-31 (NCEI Accession 0173214), NOAA National Centers
543 for Environmental Information. <https://doi.org/10.7289/v5ng4nzz>, 2018i.

544
545 Cotroneo, Y., Budillon, G., Bergamasco, A., De Alteris, A., De Stefano, M., Ferrara, C., et al.: Water
546 temperature from XBT taken from the research vessel *Italica* in the Southern Ocean and Southwest
547 Pacific Ocean from 2003-01-06 to 2003-01-11 (NCEI Accession 0173338), NOAA National Centers
548 for Environmental Information. <https://doi.org/10.7289/v5qz289c>, 2018j.

549



550 Cotroneo, Y., Budillon, G., Ferrara, C., Monteduro, R., Russo, A., & Spezie, G.: Water temperature
551 from XBT taken from the research vessel *Italica* in the Southern Ocean and Southwest Pacific Ocean
552 from 2003-12-24 to 2003-12-28 (NCEI Accession 0173328), NOAA National Centers for
553 Environmental Information. <https://doi.org/10.7289/v5vq3113>, 2018k.

554

555 Cotroneo, Y., Budillon, G., Aliani, S., Capello, M., Ferrara, C., Paschini, E. & Spezie, G.: Water
556 temperature from XBT taken from the research vessel *Italica* in the Southern Ocean and Southwest
557 Pacific Ocean from 2005-01-01 to 2005-01-06 (NCEI Accession 0173533), NOAA National Centers
558 for Environmental Information. <https://doi.org/10.7289/v5vh5m45>, 2018l.

559

560 Cotroneo, Y., Budillon, G., Ferrara, C., Meloni, R., & Spezie, G.: Water temperature from XBT taken
561 from the research vessel *Italica* in the Southern Ocean and Southwest Pacific Ocean from 2007-02-
562 05 to 2007-02-10 (NCEI Accession 0174709). Version 1.1, NOAA National Centers for
563 Environmental Information. <https://doi.org/10.25921/c8bm-xh74>, 2018m.

564

565 Cotroneo, Y., Budillon, G., Aliani, S., Ferrara, C., Greco, A., Meloni, R. & Spezie, G.: Water
566 temperature from XBT taken from the research vessel *Italica* in the Southern Ocean and Southwest
567 Pacific Ocean from 2008-01-16 to 2008-01-21 (NCEI Accession 0174711), Version 1.1. NOAA
568 National Centers for Environmental Information. <https://doi.org/10.25921/q29v-c980>, 2018n.

569

570 Cotroneo, Y., Budillon, G., Meloni, R., Aliani, S., Zambardino, G., & Spezie, G.: Water temperature
571 data from XBT taken from research vessel *Italica* in the Southern Ocean and Southwest Pacific Ocean
572 from 2010-01-25 to 2010-01-29 (NCEI Accession 0167835), NOAA National Centers for
573 Environmental Information. <https://doi.org/10.7289/v50r9mmm>, 2017a.

574

575 Cotroneo, Y., Budillon, G., Castagno, P., De Alteris, A., De Stefano, M., Falco, P., et al.: Water
576 temperature from XBT taken from research vessel *Italica* in the Southern Ocean and Southwest
577 Pacific Ocean from 2012-01-13 to 2012-01-19 (NCEI Accession 0167834). NOAA National Centers
578 for Environmental Information. <https://doi.org/10.7289/v54j0cbw>, 2017b.

579

580 Cotroneo, Y., Budillon, G., Castagno, P., Colizza, E., Cotterle, D., Falco, P., et al.: Water temperature
581 from XBT taken from the research vessel *Araon* in the Southern Ocean and Southwest Pacific Ocean
582 from 2013-01-24 to 2013-02-06 (NCEI Accession 0174794). Version 1.1, NOAA National Centers
583 for Environmental Information. <https://doi.org/10.25921/9YTS-P771>, 2018o.

584

585 Cotroneo, Y., Budillon, G., Falco, P., Fusco, G., et al.: Water temperature from XBT taken from the
586 research vessel *Italica* in the Southern Ocean and Southwest Pacific Ocean from 2006-01-01 to 2006-
587 01-04 (NCEI Accession 0207044). NOAA National Centers for Environmental Information.
588 <https://doi.org/10.25921/hzcp-d813>, 2019.

589

590 Cotroneo, Y., Ferola, A.I., Aulicino, G., Castagno, P. et al.: Water temperature taken by XBT from
591 the research vessel *Italica* in the Southern Ocean (> 60 degrees South) and Southwest Pacific Ocean
592 (limit-147 E to 140 W) from 2013-12-30 to 2014-02-18 (NCEI Accession 0287161). NOAA National
593 Centers for Environmental Information. <https://doi.org/10.25921/220j-b370>, 2024a.

594



595 Cotroneo, Y., Ferola, A.I., Aulicino, G., Castagno, P. et al.: Water temperature taken by XBT from
596 the research vessel Araon in the Southern Ocean (> 60 degrees South) and Southwest Pacific Ocean
597 (limit-147 E to 140 W) from 2015-01-02 to 2015-01-10 (NCEI Accession 0287162). NOAA National
598 Centers for Environmental Information. <https://doi.org/10.25921/9ph6-c102>, 2024b.

599

600 Cotroneo, Y., Ferola, A.I., Aulicino, G., Castagno, P. et al.: Water temperature taken by XBT from
601 the research vessel Italica in the Southern Ocean (> 60 degrees South) and Southwest Pacific Ocean
602 (limit-147 E to 140 W) from 2016-01-16 to 2016-01-28 (NCEI Accession 0287159). NOAA National
603 Centers for Environmental Information. <https://doi.org/10.25921/zf04-ch06>, 2024c.

604

605 Cotroneo, Y., Ferola, A.I., Aulicino, G., Castagno, P. et al.: Water temperature taken by XBT from
606 the research vessel Italica in the Southern Ocean (> 60 degrees South) and Southwest Pacific Ocean
607 (limit-147 E to 140 W) from 2016-12-31 to 2017-01-05 (NCEI Accession 0287163). NOAA National
608 Centers for Environmental Information. <https://doi.org/10.25921/vvmp-rr55>, 2024d.

609

610 Cotroneo, Y., Ferola, A.I., Aulicino, G., Castagno, P. et al.: Water temperature taken by XBT from
611 the research vessel Araon in Southern Oceans (> 60 degrees South) and Southwest Pacific Ocean
612 (limit-147 E to 140 W) from 2019-02-08 to 2019-02-12 (NCEI Accession 0287554). NOAA National
613 Centers for Environmental Information. <https://doi.org/10.25921/jeee-zf77>, 2024e.

614

615 Cotroneo, Y., Ferola, A.I., Aulicino, G., Castagno, P. et al.: Water temperature taken by XBT from
616 the research vessel Laura Bassi in the Southern Ocean (> 60 degrees South) and Southwest Pacific
617 Ocean (limit-147 E to 140 W) from 2020-01-07 to 2020-01-12 (NCEI Accession 0287549). NOAA
618 National Centers for Environmental Information. <https://doi.org/10.25921/1ysg-dw94>, 2024f.

619

620 Cotroneo, Y., Ferola, A.I., Aulicino, G., Castagno, P. et al.: Water temperature taken by XBT from
621 the research vessel Laura Bassi in the Southern Ocean (> 60 degrees South) and Southwest Pacific
622 Ocean (limit-147 E to 140 W) from 2020-12-25 to 2021-01-02 (NCEI Accession 0297164). NOAA
623 National Centers for Environmental Information. <https://doi.org/10.25921/aeg5-hw87>, 2024g.

624

625 Cotroneo, Y., Ferola, A.I., Aulicino, G., Castagno, P. et al.: Water temperature taken by XBT from
626 the research vessel Laura Bassi in the Southern Ocean (> 60 degrees South) and Southwest Pacific
627 Ocean (limit-147 E to 140 W) from 2022-01-08 to 2022-01-26 (NCEI Accession 0297165). NOAA
628 National Centers for Environmental Information. <https://doi.org/10.25921/3mmd-tj60>, 2024h.

629

630 Cotroneo, Y., Ferola, A.I., Aulicino, G., Castagno, P. et al.: Water temperature taken by XBT from
631 the research vessel Laura Bassi in the Southern Ocean (> 60 degrees South) and Southwest Pacific
632 Ocean (limit-147 E to 140 W) from 2023-01-06 to 2023-01-12 (NCEI Accession 0297163). NOAA
633 National Centers for Environmental Information. <https://doi.org/10.25921/kte7-d058>, 2024i.

634

635 Cotroneo, Y., Ferola, A.I., Aulicino, G., Castagno, P. et al.: Water temperature taken by XBT from
636 the research vessel Laura Bassi in the Southern Ocean (> 60 degrees South) and Southwest Pacific
637 Ocean (limit-147 E to 140 W) from 2024-01-07 to 2024-01-12 (NCEI Accession 0297166). NOAA
638 National Centers for Environmental Information. <https://doi.org/10.25921/jc13-ek97>, 2024l.

639



- 640 Cowley, R., Wijffels, S., Cheng, L., Boyer, T. and Kizu, S.: Biases in expendable bathythermograph
641 data: A new view based on historical side-by-side comparisons. *J. Atmos. Oceanic Technol.*, 30,
642 1195–1225, <https://doi.org/10.1175/JTECH-D-12-00127.1>, 2013.
- 643
644 Cowley, R. and Krummel, L. Australian XBT Quality Control Cookbook Version 2.1 (updated
645 August 2023). CSIRO, Australia. <https://doi.org/10.25919/3tm5-zn80>, 2022.
- 646
647 Daneshzadeh, Y.H., Festa, J.F. and Minton, S.M.: Procedures used at AOML to quality control real
648 time XBT data collected in the Atlantic Ocean. Miami, USA, NOAA Atlantic Oceanographic and
649 Meteorological Laboratory, 44pp, <https://doi.org/10.25607/OBP-1485>, 1994.
- 650
651 Downes, S.M., Farneti, R., Uotila, P., Griffies, S.M., Marsland, S.J. et al.: An assessment of Southern
652 Ocean water masses and sea ice during 1988–2007 in a suite of interannual CORE-II simulations,
653 *Ocean Model.*, 94, 67–94, <https://doi.org/10.1016/j.ocemod.2015.07.022>, 2015.
- 654
655 Falco, P. and Zambianchi, E.: Near-surface structure of the Antarctic Circumpolar Current derived
656 from World Ocean Circulation Experiment drifter data, *J. Geophys. Res. Oceans*, 116(C5),
657 <https://doi.org/10.1029/2010JC006349>, 2011.
- 658
659 Falco, P., Castagno, P., Cotroneo, Y., Aulicino, G., Budillon, G., de Ruggiero, P., Fusco, G. and
660 Zambianchi, G.: Measurements for Oceanography. In P. Daponte et al. (eds.), *Measurement for the
661 Sea*, Springer Series in Measurement Science and Technology, [http://dx.doi.org/10.1007/978-3-030-
662 82024-4_3](http://dx.doi.org/10.1007/978-3-030-82024-4_3), 2022.
- 663
664 Ferola, A. I., Cotroneo, Y., Wadhams, P., Fusco, G., Falco, P., Budillon, G., and Aulicino, G.: The
665 Role of the Pacific-Antarctic Ridge in Establishing the Northward Extent of Antarctic Sea-Ice,
666 *Geophys. Res. Lett.*, 50(10), <https://doi.org/10.1029/2023GL104373>, 2023.
- 667
668 Frenger, I., Münnich, M., Gruber, N., and Knutti, R.: Southern Ocean eddy phenomenology, *J.
669 Geophys. Res. Oceans*, 120, 7413–7449, <https://doi.org/10.1002/2015JC011047>, 2015.
- 670
671 GEBCO Compilation Group: GEBCO 2023 Grid, [https://doi.org/10.5285/f98b053b-0cbc-6c23-
672 e053-6c86abc0af7b](https://doi.org/10.5285/f98b053b-0cbc-6c23-e053-6c86abc0af7b), 2023.
- 673
674 Gille, S. T.: Mean sea surface height of the Antarctic Circumpolar Current from GEOSAT 600 data:
675 methods and application, *J. Geophys. Res.*, 99, 18255–18273, <https://doi.org/10.1029/94JC01172>,
676 1994.
- 677
678 Goni, G., and coauthors: More than 50 years of successful continuous temperature section
679 measurements by 943 the global expendable bathythermograph network, its integrability, societal
680 benefits, and future. *Front. Mar. Sci.*, 6:452, <https://doi.org/10.3389/fmars.2019.00452>, 2019.
- 681
682 Gouretski, V. and Reseghetti, F.: On depth and temperature biases in bathythermograph data:
683 Development of a new correction scheme based on analysis of a global ocean database. *Deep-Sea
684 Res. I*, 57, 812–833, <https://doi.org/10.1016/j.dsr.2010.03.011>, 2010.
- 685
686 Green, A. W.: Bulk dynamics of the expendable bathythermograph (XBT). *Deep-Sea Res.*, 31A, 415–
687 426, [https://doi.org/10.1016/0198-0149\(84\)90093-1](https://doi.org/10.1016/0198-0149(84)90093-1), 1984.
- 688
689 Intergovernmental Oceanographic Commission (2013) *Ocean Data Standards Volume 3.
690 Recommendation for a Quality Flag Scheme for the Exchange of Oceanographic and Marine*



- 691 Meteorological Data. Paris, France, UNESCO-IOC, 5pp. & Annexes. Intergovernmental
692 Oceanographic Commission Manuals and Guides, Vol. 54(3). <http://dx.doi.org/10.25607/OBP-6>.
693
- 694 McGillicuddy Jr, D. J.: Mechanisms of physical-biological-biogeochemical interaction at the oceanic
695 mesoscale, *Ann. Rev. Mar. Sci.*, 8, 125-159, [https://doi.org/10.1146/annurev-marine-010814-](https://doi.org/10.1146/annurev-marine-010814-015606)
696 015606, 2016.
697
- 698 Menna, M., Cotroneo, Y., Falco, P., Zambianchi, E., Di Lemma, R., Poulain, P. M. and Budillon, G.:
699 Response of the Pacific Sector of the Southern Ocean to wind stress variability from 1995 to 2017, *J.*
700 *Geophys. Res. Oceans*, 125(10), <https://doi.org/10.1029/2019JC015696>, 2020.
701
- 702 Morales Maqueda, M. A., Willmott, A. J. and Biggs, N. R. T.: Polynya dynamics: A review of
703 observations and modelling, *Rev. Geophys.*, 42.1, <https://doi.org/10.1029/2002RG000116>, 2004.
704
- 705 Orsi, A. H., Whitworth, T., and Nowlin, W. D.: On the meridional extent and fronts of the Antarctic
706 circumpolar current, *Deep-Sea Res. I*, 42(5), 641–673, [https://doi.org/10.1016/0967-0637\(95\)00021-](https://doi.org/10.1016/0967-0637(95)00021-W)
707 W, 1995.
708
- 709 Parks, J., Bringas, F., Cowley, R., Hanstein, C., Krummel, L., Sprintall, J., Cheng, L., Cirano, M.,
710 Cruz, S., Goes, M., Kizu, S. and Reseghetti, F.: XBT operational best practices for quality assurance,
711 *Front. Mar. Sci.*, 9, 991760, [https://doi.org.10.3389/fmars.2022.991760](https://doi.org/10.3389/fmars.2022.991760), 2022
712
- 713 Reverdin, G., Marin, F. Bourles, B. and L’Herminier, P.: XBT temperature errors during French
714 research cruises (1999–2007). *J. Atmos. Oceanic Technol.*, 26, 2462–2473,
715 <https://doi.org/10.1175/2009JTECHO655.1>, 2009.
716
- 717 Rintoul, S. R., Donguy, J. R., and Roemmich, D. H.: Seasonal evolution of upper ocean thermal
718 structure between Tasmania and Antarctica. *Deep-Sea Res. I*, 44(7), 1185-1202,
719 [https://doi.org/10.1016/S0967-0637\(96\)00125-2](https://doi.org/10.1016/S0967-0637(96)00125-2), 1997.
720
- 721 Rintoul, S. R.: The global influence of localized dynamics in the Southern Ocean, *Nature*, 558, 209–
722 218, <https://doi.org/10.1038/s41586-018-0182-3>, 2018.
723
- 724 Roemmich, D., Wilson, W.S., Gould, W.J., Owens, W.B., Le Traon, P.-Y., Freeland, H.J., King,
725 B.A., Wijffels, S., Sutton, P.J.H., Zilberman, N.: Chapter 4 - The Argo Program, In *Science of*
726 *Sustainable Systems, Partnerships in Marine Research*, Auad, G. and Wiese F.K. (eds), Elsevier, 53-
727 69, <https://doi.org/10.1016/B978-0-323-90427-8.00004-6>, 2022.
728
- 729 Schlitzer, R. Ocean Data View, <http://odv.awi.de>, 2011.
730
- 731 Seaver, G.A. and Kuleshov, S.: Experimental and analytical error of the expendable
732 bathythermograph. *J. Phys. Oceanogr.*, 12, 592–600, [https://doi.org/10.1175/1520-](https://doi.org/10.1175/1520-0485(1982)012<0592:EAAEOT.2.0.CO;2)
733 0485(1982)012,0592:EAAEOT.2.0.CO;2, 1982.
734
- 735 Seo, H., O’Neill, L. W., Bourassa, M. A., Czaja, A., Drushka, K., Edson, J. B., Fox-Kemper, B.,
736 Frenger, I., Gille, S. T., Kirtman, B. P., Minobe, S., Pendergrass, A. G., Renault, L., Roberts, M. J.,
737 Schneider, N., Small, R. J., Stoffelen, A., and Wang, Q.: Ocean Mesoscale and Frontal-Scale Ocean–
738 Atmosphere Interactions and Influence on Large-Scale Climate: A Review, *J. Climate*, 36(7), 1981-
739 2013. <https://doi.org/10.1175/JCLI-D-21-0982.1>, 2023.
740



- 741 Simoncelli, S., Reseghetti, F., Fratianni, C., Cheng, L., and Raiteri, G.: Reprocessing of XBT profiles
742 from the Ligurian and Tyrrhenian seas over the time period 1999–2019 with full metadata upgrade,
743 Earth Syst. Sci. Data Discuss., <https://doi.org/10.5194/essd-2023-525>, in review, 2024.
744
- 745 Sokolov, S. and Rintoul, S. R.: Circumpolar structure and distribution of the Antarctic circumpolar
746 current fronts: 2. Variability and relationship to sea surface height, *J. Geophys. Res.*, 114(C11),
747 C11019, <https://doi.org/10.1029/2008JC005248>, 2009b.
748
- 749 Sokolov, S. and Rintoul, S. R.: Circumpolar structure and distribution of the Antarctic Circumpolar
750 Current fronts: 1. Mean circumpolar paths, *J. Geophys. Res.*, 114(C11), C11018,
751 <https://doi.org/10.1029/2008jc005108>, 2009a.
752
- 753 Sokolov, S. and Rintoul, S. R.: Multiple Jets of the Antarctic Circumpolar Current South of Australia,
754 *J. Geophys. Res.*, 37, <https://doi.org/10.1175/JPO3111.1>, 2007.
755
- 756 Tan, Z., Cheng, L., Gouretski, V., Zhang, B., Wang, Y., Li, F. and Zhu, J.: A new automatic quality
757 control system for ocean profile observations and impact on ocean warming estimate, *Deep-Sea Res.*
758 *I*, 194, 103961, <https://doi.org/10.1016/j.dsr.2022.103961>, 2023.
759
- 760 Trani, M., Falco, P. and Zambianchi, E.: Near-surface eddy dynamics in the Southern Ocean, *Polar*
761 *Research*, 30(1), 11203. <https://doi.org/10.3402/polar.v30i0.11203>, 2011.
762
- 763 Trani, M., Falco, P., Zambianchi, E., and Sallee, J. B.: Aspects of the Antarctic Circumpolar Current
764 dynamics investigated with drifter data, *Prog. Oceanogr.*, 125, 1–15,
765 <https://doi.org/10.1016/j.pocean.2014.05.001>, 2014.
766